APPLIED SCIENCES AND ENGINEERING

Plant electrophysiology with conformable organic electronics: Deciphering the propagation of Venus flytrap action potentials

Adam Armada-Moreira[1,2]†, Abdul Manan Dar[1]†, Zifang Zhao[3], Claudia Cea[3], Jennifer Gelinas[4], Magnus Berggren[1,5], Alex Costa[6,7], Dion Khodagholy[3]*, Eleni Stavrinidou[1,5,8]*

Electrical signals in plants are mediators of long-distance signaling and correlate with plant movements and responses to stress. These signals are studied with single surface electrodes that cannot resolve signal propagation and integration, thus impeding their decoding and link to function. Here, we developed a conformable multielectrode array based on organic electronics for large-scale and high-resolution plant electrophysiology. We performed precise spatiotemporal mapping of the action potential (AP) in Venus flytrap and found that the AP actively propagates through the tissue with constant speed and without strong directionality. We also found that spontaneously generated APs can originate from unstimulated hairs and that they correlate with trap movement. Last, we demonstrate that the Venus flytrap circuitry can be activated by cells other than the sensory hairs. Our work reveals key properties of the AP and establishes the capacity of organic bioelectronics for resolving electrical signaling in plants contributing to the mechanistic understanding of long-distance responses in plants.

INTRODUCTION

Electrical signals in plants are nowadays well-recognized information carriers with direct functional relevance. These signals are often correlated to thigmonastic movements (1, 2) and responses to stress, including touch, (herbivore-induced) wounding (3–5), and root nematode attack (6, 7). Specifically, severe wounds induce slow wave potentials, which are varying amplitude depolarizations that usually last for few minutes (8). In carnivorous plants, stimulation of mechanosensitive cells (e.g., sensory hairs) induces fast electrical transients called action potentials (APs) that are usually correlated with rapid movements. A key example of plant AP occurs within the carnivorous plant Venus flytrap (VFT; *Dionaea muscipula*), and it is considered a model system for fast electrical signaling in plants (9). Despite the importance of these signals, our understanding of their properties, underlying mechanisms, and precise relationship with plant function remains incomplete. A major barrier to addressing these issues is that plant electrophysiology has thus far mainly relied on cumbersome intracellular recordings (10) or noninvasive surface recordings with bulky inorganic (Ag/AgCl) electrodes, neither of which enable high-resolution mapping of the signal (11, 12).

The signal characteristics of the VFT have been mainly studied with noninvasive surface Ag/AgCl electrodes. AP in VFT is generated after the stimulation of one of the six sensory hairs present in the inner side of the trap (13). The AP has a diphasic shape, with a fast depolarization phase followed by a more variable hyperpolarization (10, 14), a signal amplitude between 10 and 150 mV, and a signal duration of 1 to 3 s (15–20). Several studies have attempted to estimate the propagation speed of the AP in VFT with the use of electrode pairs, and, so far, a wide range of values have been reported in the literature ranging between 2 and 80 cm s^{-1} (15, 19–21), suggesting a lack of consensus approach to such measurements. If any two of the hairs of the VFT are stimulated within an interval of 30 s, then the trap closes, showcasing a highly regulated biological phenomenon, designed to optimize yield of nutrition for the plant. However, the causal mechanisms triggering trap closure are unclear.

A long-lasting hypothesis was that the AP induces a transient increase in calcium ions (Ca^{2+}) concentration in the trap and when the Ca^{2+} concentration reaches a putative threshold the trap closure is triggered. Recently, a major milestone has been achieved with the generation of VFT transgenic plants that express the fluorescent Ca^{2+} indicator GCaMP6f, enabling visualization of the Ca^{2+} dynamics in intact traps (22). The hypothesis was confirmed since the mechanical stimulation of the sensitive hairs led to an increase in cytosolic Ca^{2+} at the base of the hair. The Ca^{2+} transient then spread throughout the trap with a time constant of 33 s (14, 22), and, when a second stimulation was applied within 30 s, a second higher Ca^{2+} transient was generated and the trap closed. The cytosolic Ca^{2+} concentration level is probably the main "memory" component of the trap, while its proper decoding seems to be necessary to elicit closure (23). While the transgenic VFT enables the visualization of the Ca^{2+} wave propagation, the AP is an integrated signal involving the activity of more than one type of ion channel with different permeabilities for different ions such as Ca^{2+}, K$^+$, Cl$^-$, and H$^+$, each being a component of the AP (14). However, up to now,

[1]Laboratory of Organic Electronics, Department of Science and Technology, Linköping University, SE-601 74 Norrköping, Sweden. [2]Neuronal Dynamics Lab, International School for Advanced Studies, 34136 Trieste TS, Italy. [3]Department of Electrical Engineering, Columbia University, New York, NY 10027, USA. [4]Department of Neurology, Columbia University Medical Center, New York, NY 10032, USA. [5]Wallenberg Wood Science Center, Department of Science and Technology, Linköping University, SE-601 74 Norrköping, Sweden. [6]Department of Biosciences, University of Milan, 20133 Milano, Italy. [7]Institute of Biophysics, National Research Council of Italy (CNR), 20133 Milano, Italy. [8]Umeå Plant Science Center, Department of Forest Genetics and Plant Physiology, Swedish University of Agricultural Sciences, SE-901 83 Umeå, Sweden.
*Corresponding author. Email: dk2955@columbia.edu (D.K.); eleni.stavrinidou@liu.se (E.S.)
†These authors contributed equally to this work.

the different ionic components of the AP have not been fully decoupled. Furthermore, how the AP propagates along the trap and how its propagation correlates with Ca^{2+} wave propagation or other ions and mobile signaling molecules or with the trap closure per se remain unknown.

Advancements in bioelectronics have resulted in the development of noninvasive electrophysiological recording devices for mammalian systems, enabling unprecedented spatiotemporal resolution and critical insight into neural circuit mechanisms (24–26). Systems based on conformable, low-impedance multielectrode arrays (MEAs) permitted recording and classification of individual neural APs from the surface of human and rodent brains (27, 28). To the best of our knowledge, there are only three studies that used MEA technology interfaced with plant tissues: root slices (29) and leaves of intact plants (15, 30). In a recent study, a small-scale rigid MEA was used in VFT; however, the study mainly focused on the calculation of conduction velocity (15). Other recent examples in literature also demonstrate AP recordings with conformable tattoo-like single electrodes based on organic electronic materials (31) or nanomaterials (32) and with single organic electrochemical transistors that enable signal amplification (16, 33). However, these studies did not provide any new insight on the AP but focused on the device development.

In this work, we developed a conformable MEA based on organic electronics for large-scale and high-resolution plant electrophysiology. With these devices, we performed precise spatiotemporal mapping of the VFT AP and demonstrated that it is actively propagating through the tissue in nonclosure- and closure-inducing events. We correlate the electrical signals to trap movement and resolve the origin of spontaneously generated APs. We also found that cells other than the sensory hairs could generate AP that can also lead to trap closure. Last, with pharmacological treatments, we investigate the role of ions on the AP propagation. Our work establishes the capacity of organic bioelectronic devices for high-resolution and large-scale plant electrophysiology that can contribute to the mechanistic understanding of electrical signaling in plants.

RESULTS

We developed a NeuroGrid probe with 20 mm by 25 mm spatial coverage using 120 uniformly distributed conducting polymer-based electrodes (500 μm by 500 μm; Fig. 1A). The conformability of the NeuroGrid is an essential feature for large-scale electrophysiology recordings as it allows the MEA to follow the trap curvature, both in open and closed states, without displacement (Fig. 1B). To record the AP propagation in the VFT trap, we simply laminated the NeuroGrid to the outer surface of the lobe, to avoid triggering of the mechanosensitive hairs, with a small amount of electrolyte between the recording electrodes and plant tissue (Fig. 1C). Stimulating of one hair resulted in AP generation and propagation that we could track across the lobe (Fig. 1Di). A clear signal delay between the recordings of the different electrodes was observed, indicating that our setup has sufficient spatial and temporal resolution to resolve the signal propagation. The time delay was then quantified as the time difference between the signal of each electrode and the first signal recorded, allowing for the generation of the time delay AP propagation map (Fig. 1Dii). As the relative position of the sensitive hairs in relation to the electrodes can be visually estimated, this analysis enabled us to independently confirm that the AP originates

at the vicinity of the stimulated hair. These conclusions were then corroborated by phase shift analysis. The phase of each signal was estimated by a Morlet wavelet centered on 1.14 Hz, representing the main frequency content of the AP signal (figs. S1 and S2). The phase shift of the waveform mapping matched the one of time delay, indicating that the waveform of the AP travels without losing its frequency content. (Fig. 1Diii).

Since the AP originates at the hair, it is important to investigate whether the signal delay recorded by the other electrodes is not due to volume conduction (i.e., recording of a localized signal through an electrolytic medium) but a result of active propagation of the signal through the tissue. To test this, we applied an electrical stimulus on the trap using an external Ag/AgCl electrode and recorded the signal with the NeuroGrid (Fig. 1Ei). In this case, the stimulation artifact was recorded by all electrodes without notable time delay or phase shift, confirming that the electrical stimulation does not propagate but can be captured from all electrodes simultaneously due to sufficient ionic conductivity of the epidermal tissue (Fig. 1Eii). In contrast, the time delay of the AP propagation and the phase shift mapping suggest that the AP travels through compartmentalized pathways, however without dampening of the signal indicating an active propagation.

To map the signal propagation across the whole lobe, we repeated the same experimental protocol with different grid placements with respect to the sensory hairs (H1, H3, and H6) (Fig. 2A). We found that the signal traveled with constant speed for all the hairs with similar average speed (table S1 and fig. S3). The propagation maps were then calculated with isochronal lines and show that the signal is generated at the hair location, and it radially spreads to the rest of the trap without strong directionality (Fig. 2A). As H6 is on the opposite lobe from the grid, the signal origin on the map corresponds to the area just above the midrib location closer to H6, clearly showing that the signal propagates to both lobes. A second stimulation of the trigger hair was then performed, with at least 1 min of interval to prevent trap closure (Fig. 2B). In all cases, the AP propagated more quickly after the second stimulation (preexcited state) compared to the first stimulation (nonexcited state), 11.22 ± 0.82 cm s^{-1} versus 41.14 ± 2.39 cm s^{-1}, respectively (Fig. 2C and table S1). Several studies have attempted to estimate the propagation speed of this signal, with most works suggesting a speed of 10 to 80 cm s^{-1} (15, 19–21). Other studies present conflicting propagation speeds, from 2 cm s^{-1} (14) to 10 m s^{-1} (34). However, previous studies relied on electrode pairs without the possibility to extract information about the speed dependence with time and the directionality of the signal. Here, we provide a better estimation for the propagation speed and show that the propagation speed is constant, with no strong directionality. Together with the propagation of the AP, a slower Ca^{2+} transient spreads throughout the trap, with a speed of c. 2 cm s^{-1} (14, 22), as it was visualized in VFT expressing the GCaMP6f genetically encoded Ca^{2+} indicator. They found that the Ca^{2+} wave travels faster (5 cm s^{-1}) toward the midrib than in the other directions (2 cm s^{-1}) and that, similarly to the AP propagation, the Ca^{2+} wave speed following the second stimulation increases two- to threefold (22). In a following study, it was also suggested that the speed of the AP in nonexcited traps is the same as the one of the Ca^{2+} transient (14). According to our results, the AP propagates much faster than the Ca^{2+} transient and without strong directionality. Our results therefore suggest that the AP precedes the spread of the Ca^{2+} transient.
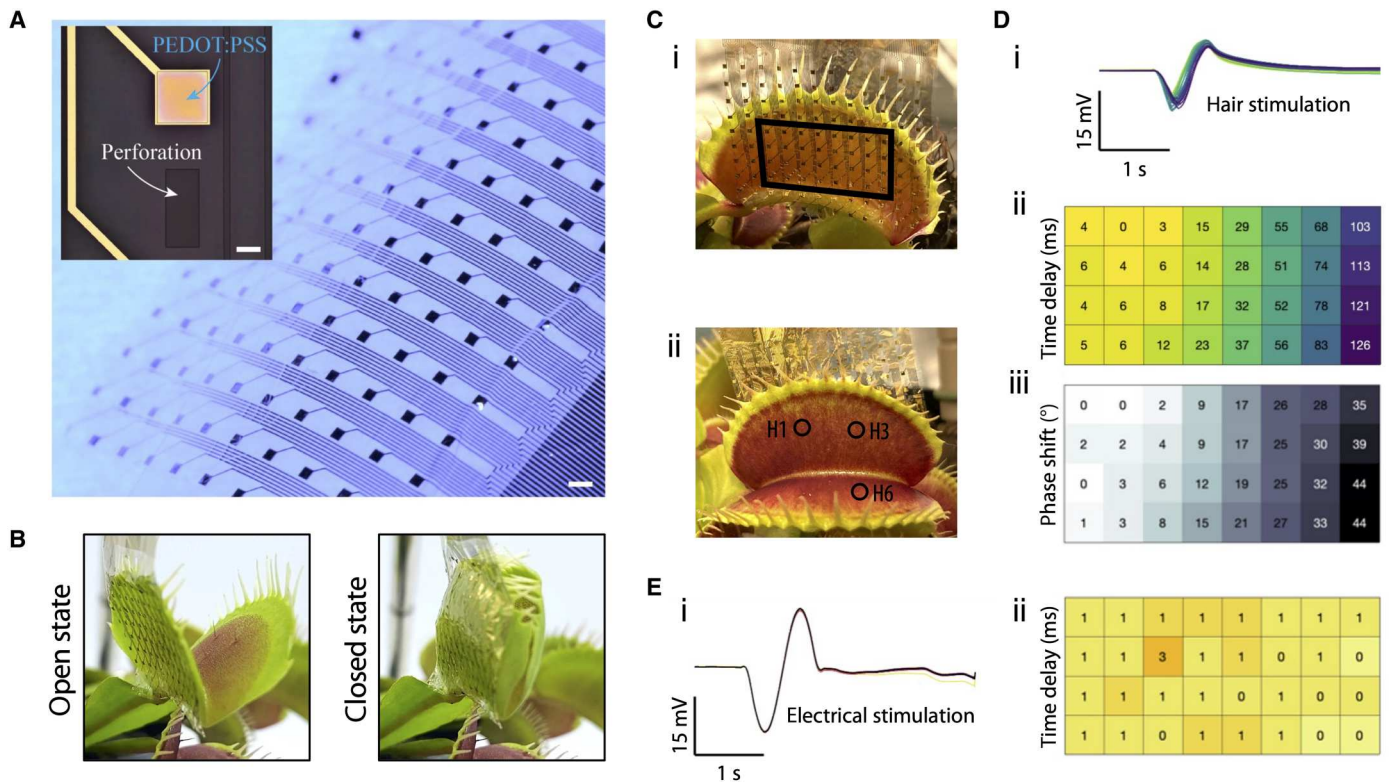
Fig. 1. The AP propagates along the trap and is resolved with high spatiotemporal resolution. (**A**) NeuroGrid MEA with an interelectrode distance of 2 mm. Scale bar, 1 mm. Inset shows a PEDOT:PSS/Au electrode of 500 μm by 500 μm. Scale bar, 250 μm. (**B**) The conformatibility of the NeuroGrid allows it to follow the curvature of the VFT trap in the open and closed states. (**C**) The NeuroGrid is attached to the lobe outer side of a VFT using electrolyte. The black square represents the active recording electrodes (i). Three hairs are localized in relation to the NeuroGrid, H1 closer to the petiole, H3 further away, and H6 contralateral to the NeuroGrid (ii). (**D**) H1 was mechanically stimulated, leading to the recording of the generated AP (i). By analyzing the time delay in each electrode, it is possible to create a spatiotemporal propagation map (ii). This map was corroborated by phase shift analysis (iii). (**E**) In contrast, when the trap is electrically stimulated from an external source (i), the stimulation artifact shows no signal propagation (ii).

After establishing the propagation of the signal, we analyzed in more detail the AP waveforms, considering the signals recorded by the electrode closest to the stimulated hairs. We observed that the waveforms of H1 and H3 have very similar characteristics, while, in the one recorded from H6, a small hyperpolarization is present (Fig. 2D). This difference is likely related to the position of H6, in which it is on the opposite lobe of the recording electrodes. Furthermore, when comparing the first and second stimulations of the same trigger hair, there is an increase in amplitude in the latter (Fig. 2D) that, although not statistically significant, had already been previously noted (*35*). In addition, we observe that the time interval between the mechanical stimulation of the hair and the onset of the AP decreases for the second stimulation (Fig. 2E, i and ii). However, while the AP occurs faster, the depolarization time remains unchanged between the first and the second stimulations (Fig. 2Eiii). Together, these data indicate that the second AP is facilitated by the first AP, leading to a faster electrical response while maintaining its signal characteristics.

The relationship between electrical activity and trap movement was then explored by simultaneously recording electrical responses and acquiring video (Fig. 3A). In these experiments, a second stimulation was provided within 30 s of the first stimulation to trigger trap closure. Despite having significant natural deformation and movement of the lobe during trap closure, no motion-induced

artifacts were observed (fig. S4). We found that the time difference between the AP onset and initiation of trap movement was 472 ± 24.7 ms (means ± SEM, *n* = 19) and that the closing movement lasted 1408 ± 157.1 ms (means ± SEM, *n* = 27), both are in line with previous reports (*35–37*). We also found that the trap movement onset is delayed by 12 ms/s of interval between the first and the second stimulations (fig. S5), which is likely related to the decay of the Ca^{2+} transient that accompanies the AP propagation (*22*). The recorded signals during the second stimulation were diverse (Fig. 3B), having either simple (only one AP) or complex features where spontaneous AP (one or more) was generated after the mechanostimulated AP. The complexity of the recorded signal is significantly correlated with the interval between the first and the second stimulations, with complex responses being associated with larger intervals and simple responses being associated with smaller ones (Fig. 3C). Unexpectedly, we found that the spontaneous AP typically originated from an unstimulated hair (*n* = 5; Fig. 3, E and F, and fig. S6). In c. 60% of the complex responses, we observed that the trap was slowly closing before the occurrence of spontaneous AP and that the propagation of this spontaneous AP subsequently accelerated trap closure (Fig. 3B). One speculation is that the spontaneous AP is generated to induce more Ca^{2+} release to pass the putative threshold that will lead to trap closure.
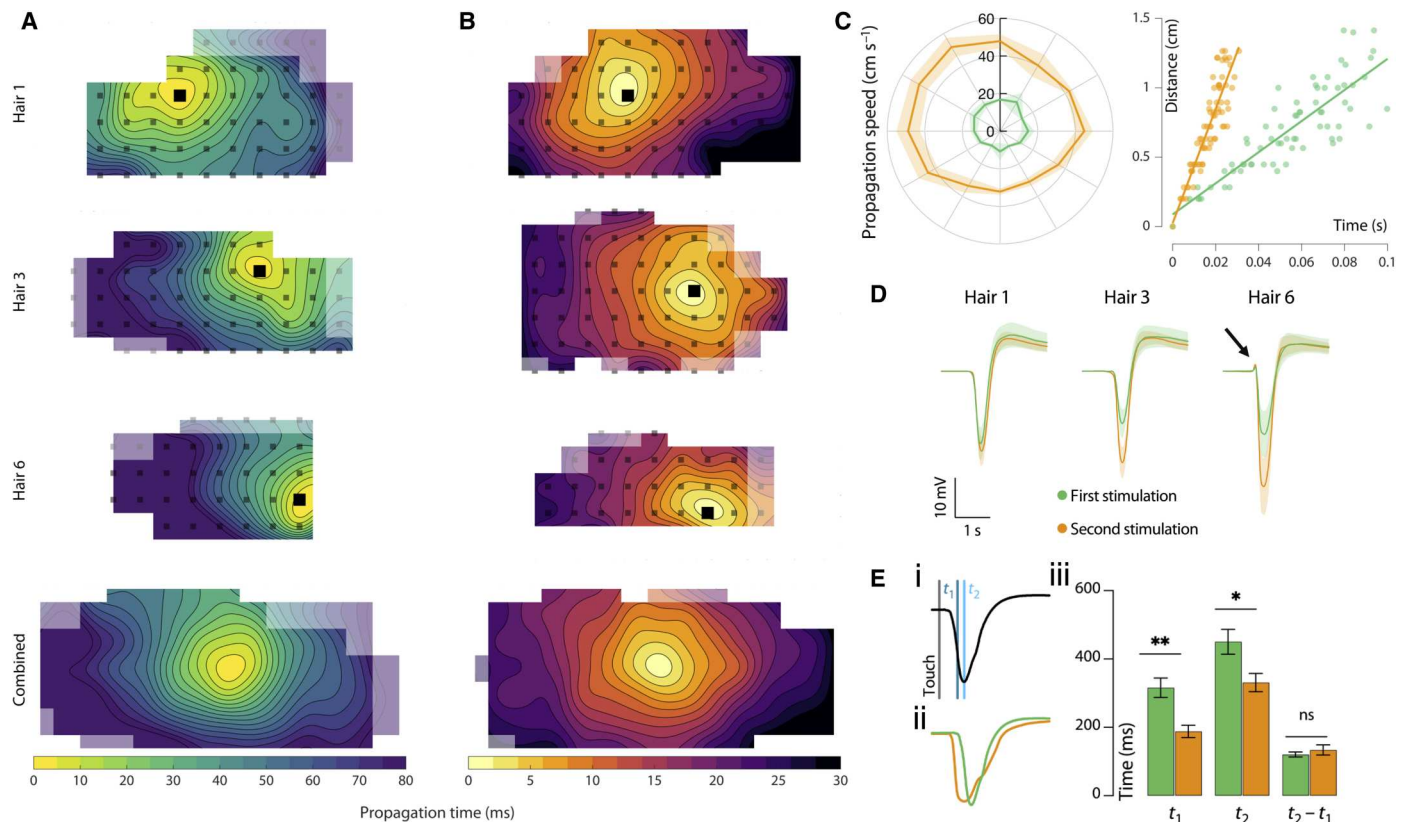
Fig. 2. AP propagates radially along the lobe with second stimulation being facilitated by the first one. From the stimulation of the different trigger hairs, the average AP propagation maps for the (**A**) first and (**B**) second stimulations were obtained. All experiments were aligned on the basis of electrode origin. Pixel transparency relates to number of independent experiments that contributed to its values, where $n = 0$ to 1 for white, $n = 2$ for 50% transparency, and $n \geq 3$ for full color. $n = 6$ to 22. Isochronal lines for first stimulation = 5 ms. Isochronal lines for second stimulation = 2 ms. Electrode placement represented with black pixels, with an interelectrode distance of 2 mm. (**C**) The AP during first (green) and second (orange) stimulations travels radially with no strong directionality, as shown by the propagation speed in different directions (left, means ± SD) (right, scatter plot for all directions together). (**D**) Comparison of AP waveform obtained by triggering different hairs and between first and second stimulations for each hair. Significantly different specific features of H6 stimulation were shown with black arrow. Data represented as means ± SEM. $n = 7$ to 21. (**E**) The time delays (i) from touch to maximum of first derivative (t_1) and to AP minimum (t_2) were quantified for the first and second stimulations. (ii) Overlayed action potentials recorded in the first and second stimulations of the same trap. (iii) Both time delays decrease in the second stimulation, while the AP depolarization time ($t_2 - t_1$) remains unchanged. $n = 20$ to 22. *$P < 0.05$ and **$P < 0.01$ using mixed-effects analysis followed by Sidak's multiple comparisons test. ns, not significant.

So far, we monitored the AP propagation originating from mechanosensitive hairs. Previous studies have shown that wounding the VFT lobe also generates an AP, although without elucidating the origin of these APs (*38*). To investigate the origin and properties of wound-induced AP, we established a wounding assay using a low-power laser focused on a specific location on the inner part of the lobe, far from the mechanosensitive hairs (Fig. 4, A and B). The mechanostimulation of the hair induced an AP at the hair location (Fig. 4C, i and ii), whereas wounding induced an AP originating at the wound site ($n = 4$; Fig. 4Ciii and fig. S7). Furthermore, when stimulating twice with the laser, the trap closed and, on some occasions, a spontaneous AP arose, originating from a different location, probably a hair location ($n = 2$; Fig. 4D and fig. S8). These experiments indicate that the activation of the VFT trap circuitry is not restricted to the sensory hairs, but it is extended to other cells where excitations can also be integrated and lead to movement.

To examine the roles of the specific ions involved in the AP generation and propagation, we used a pharmacological approach with ion channel blockers. In line with previously described protocols (*14*, *39*, *40*), we immobilized a trap and excised one lobe to apply

the blockers at the wounded site. In this configuration, it is necessary to record the AP from the inside of the trap. Therefore, we first verified that recordings from the inside and the outside of a trap are equivalent (Fig. 5A). We then used a smaller, commercially available high-resolution MEA (FlexMEA) to map the AP from the inside of the trap. In this case, we also verified that the AP propagation speed is similar for recordings with FlexMEA and NeuroGrid in untreated traps (Fig. 5B).

After trap excision, the immobilized lobe was incubated with different concentrations of the Ca^{2+} channel blocker $LaCl_3$ or the K^+ channel blocker TEACl, and AP was recorded every hour using single Ag/AgCl electrodes. Notably, $LaCl_3$ is not specific to Ca^{2+}-permeable channels, and it can affect other cation channels as well. Control traps were incubated for the same amount of time with deionized (DI) water. As shown in Fig. 5C, incubation with $LaCl_3$ leads to a decrease in AP amplitude in a concentration-dependent manner, with no impact on the waveform FWHM (full width at half maximum). On the other hand, when traps were incubated with TEACl, the AP amplitude was maintained at control levels, but the FWHM increased markedly in a concentration-dependent
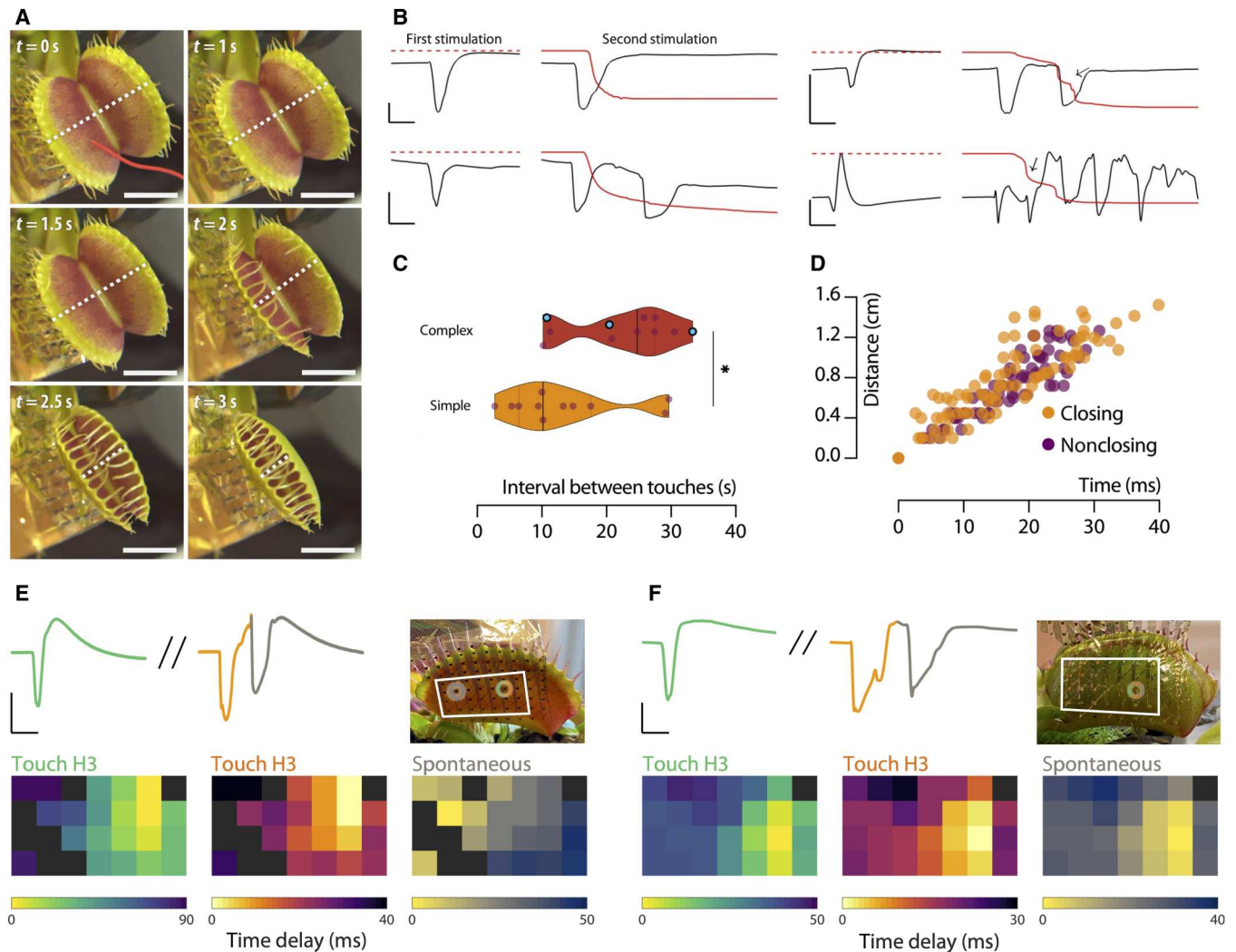
Fig. 3. Spontaneous APs that are generated in some trap closure events can originate from nonstimulated hairs and correlate with stimulation interval and movement. (**A**) Mechanically induced trap closure. One of the sensitive hairs of a VFT was mechanically stimulated, and the maximal distance between the two lobes (white dotted line) was measured during closure. Scale bars, 1 cm. Time is indicated in each frame. (**B**) Diversity of electrical activity (black trace) and movement (red trace) captured during first mechanical stimulation (no trap movement) and during second mechanical stimulation inducing trap closure. In some cases, during trap closure, spontaneous APs are generated (one or more extra APs) that sometimes correlate with shifts in movement (black arrows). X scale bars, 1 s; Y scale bars, 10 mV. Movement trace is normalized from maximum distance to closure. (**C**) More complex signals during second stimulation (two or more APs, purple and blue dots, respectively) are associated with longer intervals between touches, while simple signals (a single AP) tend to be generated with shorter intervals. *$P < 0.05$ using an unpaired t test. $n = 11$ for each group. (**D**) Scatter plot of signal propagation for second stimulation in trap closure (orange) and trap nonclosure (purple) events. (**E**) Following two stimulations of H3, a spontaneous AP is generated originating from the nonstimulated H1. Representative AP waveforms (X scale bar, 1 s; Y scale bar, 5 mV) and corresponding propagation maps. Photograph shows the grid active area and hair locations. $n = 4$. (**F**) On one occasion following two stimulations of H3, a spontaneous AP is generated from the same hair. APs waveforms (X scale bar, 1 s; Y scale bar, 5 mV) and corresponding propagation maps. Photograph shows the grid active area and hair location.

manner. These modulations of the AP waveform are in line with previous work (*14*), while we additionally perform detailed characterization of the AP over time and in response to different ion channel blocker concentrations.

Considering the time course of the tested ion channel blockers, an incubation of 3 hours with 10 mM LaCl$_3$ and that of 4 hours with 100 mM TEACl were chosen to map the signal propagation with the FlexMEA (Fig. 5D). When Ca^{2+} fluxes were perturbed (Fig. 5E), there was a decrease in AP amplitude compared to the AP baseline, but no significant differences in propagation speed (compared to control traps) were found. In contrast, when K$^+$ fluxes were

impaired (Fig. 5F), there was a significant increase in FWHM compared to the AP baseline, but no significant differences in propagation speed were found. There was a generalized decrease in propagation speed under all tested conditions compared to that measured in intact traps. This decrease likely arises from metabolic changes in the excised traps rather than effects of the ion channel blockers, as incubation with DI water induced a similar decrement in propagation speed. In summary, while the data recorded with the FlexMEA corroborates that acquired with the Ag/AgCl electrodes in terms of waveform distortion, we were unable to find any impact of
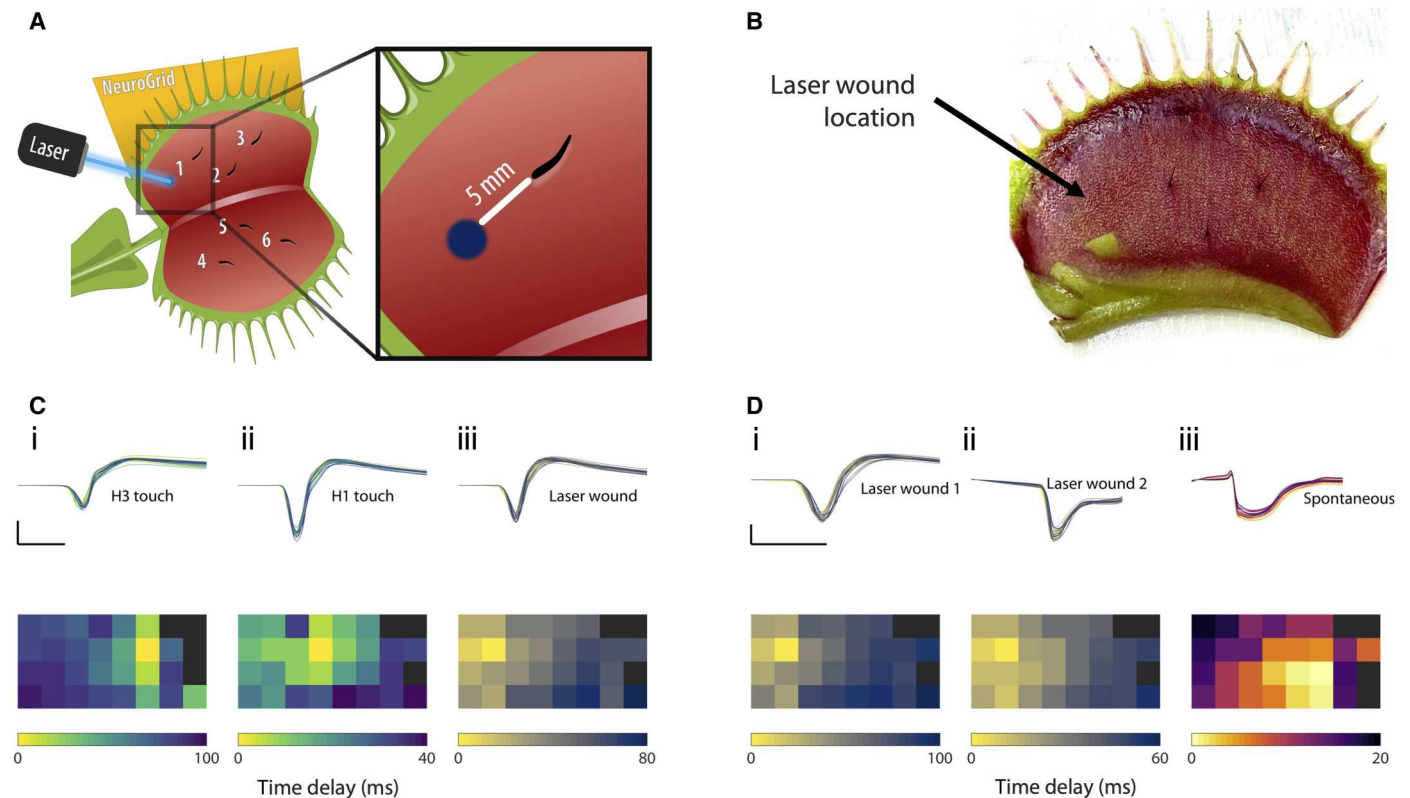
Fig. 4. VFT trap circuitry can be triggered by other cells not only the sensory hairs. (**A**) Wounding assay using a low-power laser. The laser induces a wound at a location away from sensory hairs, approximately 5 mm from H1. (**B**) Representative photograph of trap after wounding assay showing that the laser does not induce a severe wound. (**C**) Representative AP waveforms and corresponding propagation maps generated from mechanostimulation of H3 (i), H1 (ii), and the wound site (iii), clearly demonstrating the different origins of the AP in each case, $n = 4$. (**D**) Twice wound stimulation induces trap closure and spontaneous AP generation. Representative AP waveforms and corresponding propagation maps of APs generated from laser induced wound (i and ii) and spontaneous AP (iii), clearly demonstrating that the spontaneous AP originates from a location different from the wound site, $n = 2$. X scale bars, 1 s; Y scale bars, 20 mV.

the disruption of Ca^{2+} and K^+ fluxes on the spatial propagation speed of the AP.

DISCUSSION

In this work, we demonstrate the ability of conformable MEAs to elucidate properties of electrical signaling in plants. We mapped mechanostimulated AP propagation in the VFT and found that the signal travels with constant speed in both lobes and spreads radially from the hair with no strong directionality. The AP travels faster than the Ca^{2+} transient and does not follow its anisotropy [as compared with data from Suda *et al.* (*22*)], suggesting that the AP precedes the Ca^{2+} wave propagation. In preexcited traps, the AP has higher amplitude, travels faster, and occurs with less delay from the mechanostimulation event in comparison with nonexcited traps, indicating that the trap state affects the AP propagation. Furthermore, we found that in some closing events, spontaneous APs are generated that mostly originate from nonstimulated hairs. The likelihood of spontaneous AP generation is highly correlated with a longer interval between stimulations of the sensory hairs and, on some occasions, was associated with the onset of a faster trap movement during closure. The physiological role of the spontaneous AP is not clear; however, it might be generated to induce additional Ca^{2+} release that will facilitate complete closure of the trap.

What defines the speed of the AP and which tissues are involved in the AP propagation are still major questions. We demonstrate that the AP actively propagates throughout the trap, and it is not just a localized signal that can be probed from various distances through an electrolytic medium. We show that AP propagation is not directional, and, therefore, it cannot be mediated via tissues that are not homogenously distributed across the trap. The hypothesis that AP propagation occurs via the phloem vasculature (*9*) is not supported by our work because, in this case, AP propagation speed should be increased in directions aligned with phloem anatomy. In addition, pharmacological disruption of Ca^{2+} and K^+ fluxes lead to waveform distortion but did not affect the propagation speed of the AP.

Wounding assays revealed that other tissues apart from the mechanosensitive hairs are excitable. These wounded locations could generate APs that were sufficient to subsequently induce trap closure. The circuitry of the VFT trap can be therefore activated not only through the stimulation of the sensory hairs but also via disruption of other cells. In the transgenic VFT expressing the GCaMP6f Ca^{2+} indicator, it was demonstrated that cytosolic Ca^{2+} increases at the wound site that then propagates across the lobe extending the correlation between AP generation and Ca^{2+} release in cells others than the sensory ones. However, what is not clear is whether the Ca^{2+} levels of the lobe are associated with the AP
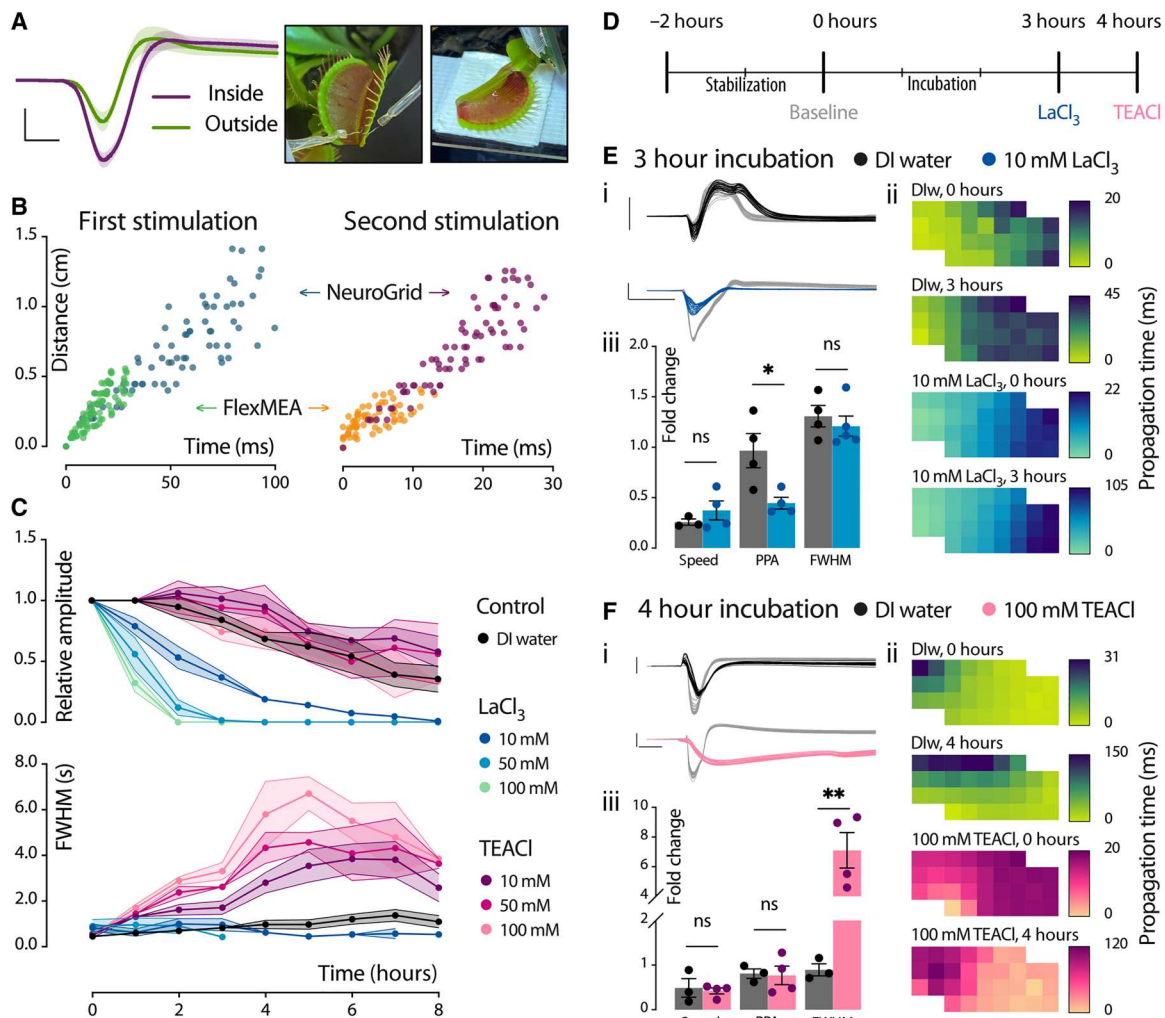
Fig. 5. Ca²⁺ and K⁺ influx do not affect AP propagation speed along the lobe. (**A**) AP recorded simultaneously from the inside and outside of the same trap, using Ag/AgCl electrodes (means ± SEM), $n = 9$. Y scale bar, 20 mV; X scale bar, 200 ms. FlexMEA can be placed on the inside of the trap. (**B**) Comparison of AP propagation recorded with FlexMEA and NeuroGrid. (**C**) Effects of treatment with Ca²⁺ channel (LaCl₃) or K⁺ channel blocker (TEACl) on AP characteristics (means ± SEM, $n = 3$ to 8). (**D**) Experimental timeline: Traps were incubated with DI water for 2 hours, and baseline APs were recorded. Then, traps were incubated with DI water or ion channel blockers, and post-treatment APs were recorded. (**E**) Effects of Ca²⁺ signal disruption on AP. (i) Representative AP for trap incubated for 3 hours with DI water or with 10 mM LaCl₃. Baseline APs are in light gray. Y scale bar, 10 mV; X scale bar, 1 s. (ii) Representative AP propagation maps for the baseline, and post-treatment recordings of a control trap and a LaCl₃-treated trap. (iii) Quantification of AP parameters, represented as fold change in relation to respective baseline AP. $n = 3$ to 5. ns, $P > 0.05$ and *$P < 0.05$ using an unpaired two-tailed t test. (**F**) Effects of K⁺ signal disruption on AP. (i) Representative AP for trap incubated for 4 hours with DI water or with 100 mM TEACl. Y scale bar, 10 mV; X scale bar, 1 s. (ii) Representative AP propagation maps for the baseline, and posttreatment recordings of a control trap and a TEACl-treated trap. (iii) Quantification of AP parameters, represented as fold change in relation to respective baseline AP. $n = 3$ to 4. ns, $P > 0.05$ and **$P < 0.01$ using an unpaired two-tailed t test.

propagation? A second stimulation of a sensory hair will lead to trap closure only when the concentration of cytosolic Ca²⁺ before the stimulation is high enough. We observed that the propagation speed of the AP during the second stimulus is faster independent whether it will lead to trap closure, signifying that it does not depend on the cytosolic Ca²⁺ concentration of the trap. This is corroborated by the results of the pharmacological treatment where blocking plasma membrane Ca²⁺-permeable channels had no impact on the AP propagation speed. Nevertheless, in the latter case, we cannot exclude the contribution of internal stores in the increase of cytosolic Ca²⁺ concentration. In addition, any combination of hair stimulations induces faster AP propagation during the

second stimulation, indicating that the excitability information must be encoded across the entire trap, rather than coupled with the stimulated hair alone. The nature of this information encoding remains unclear. Recently, in Arabidopsis, it has been shown that upon wounding glucohydrolase, enzymes generate mobile signaling molecules (e.g., Ricca's factors) and that, together with hydraulic pressure changes, they are involved in the electrical signal and Ca²⁺ wave propagation (*41*, *42*). We can only speculate that, in the VFT, similar mechanisms might be triggered upon AP generation and therefore be involved in the excitability of the trap. The existence of mobile elicitors was suggested by Ricca in studies performed in the sensitive plant Mimosa (*43*).

Our work leverages the conformability, biocompatibility, and high spatiotemporal resolution of organic electronics to shed light onto the mechanistic underpinnings of electrical signaling in plants. We resolve key properties of AP propagation across the VFT lobes, pinpoint the origin of spontaneous AP, and demonstrate that the VFT circuitry can be activated by cells other than the sensory hairs. This work also establishes the foundation for translating methods validated in mammalian electrophysiology to plant electrophysiology. The ability to spatially resolve electrophysiological signals in plants in a quantitative manner opens a range of new research possibilities. We have validated the technology for fast electrical signaling, and similar approaches can be promptly applied to resolve slower signals. Currently, there are no commercially available solutions for high-resolution or large-scale electrophysiology recording for plants. Although, in this study, we also performed recordings with a smaller commercial MEA that enabled us to record from the inside of the trap, it became apparent that this device was limited for plant recordings due to features optimized for interfacing with the rodent brain. These experiments further highlighted the need for developing customized electrophysiology platforms for plant science. High-resolution electrophysiology can be combined with genetics, and we foresee that it will enable precise quantification of even subtle changes in mutants with minor phenotypic defects, thus representing a fundamental contribution to the mechanistic understanding of long-distance signaling in plants.

MATERIALS AND METHODS

Plant material
VFT (*D. muscipula*) plants were purchased from Plantagen (Sweden), repotted in sphagnum moss:perlite (2:1) soil mixture, and kept under greenhouse conditions (22°/18°C light/dark, 12 hour photoperiod, and 60% relative humidity). Plants were watered with DI water.

NeuroGrid fabrication
One hundred–millimeter 550 μm ± 10 μm P-doped wafers were coated with 2 μm of parylene-C using an SCS Labcoater 2 to form the base layer of the NeuroGrid. Metallization was patterned using a liftoff approach. AZ nLOF 2020 photoresist was spin-coated at 3000 rpm with soft bake and postexposure baked at 110°C for 90 s each. Ultraviolet exposure was performed using a Suss MA6 DUV Mask Aligner, and samples were developed in a bath of AZ 300 MIF. An adhesion layer of 10 nm titanium was evaporated, followed by an evaporated 150 nm gold layer using a ultrahigh vacuum angstrom electron beam evaporator. Liftoff was performed using a bath of remover PG. Subsequently, a second layer of parylene-C (insulation layer), followed by an additional sacrificial layer of parylene-C (for the subsequent peel-off process), was deposited. The adhesion between the first and the second layers of parylene-C was enhanced by Silane A-174 (chemical vapor deposited), while an antiadhesion agent (5 wt % of Micro-90 diluted in DI water) reduced the adhesion between second and third layers. The stacked layers were patterned with a layer of AZ9260-positive photoresist and dry-etched with a plasma reactive ion etching (RIE) process [Oxford Plasmalab 80+; 180 W, 50 sccm (standard cubic centimeters per minute) O2, and 2 sccm SF6] to shape the electrodes and contacts. Specifically, AZ9260 was spin-coated at 5000 rpm, baked at 115°C for 90 s, exposed using a Suss MA6 Mask Aligner, and developed with AZ400K developer

(1:4 with DI water). An extra layer of AZnLOF2020 (3000 rpm; the guard photoresist) was added between the metal layer and the later parylene layers to protect Au contacts from direct ion bombardment during RIE process. The contact area of the electrodes were realized by spin-coating and baking poly(3,4-ethylenedioxythiophene):polystyrene sulfonate (PEDOT:PSS) (600 rpm) and patterned by peeling off the sacrificial parylene layer. After patterning, the wafer is cleaned thoroughly with acetone and isopropanol to remove guard photoresist and released in a water bath.

A multilayer polychlorinated biphenyl (PCB) was designed using Autodesk Eagle software to interface 32 NeuroGrid electrodes with the ME2100-System (Multichannel Systems, Germany). The NeuroGrid was attached to the 350 μm PCB connections using a mixed conducting particulate composite material anisotropic film. Last, the PCB was equipped with a 36 pin connector (1.27 mm pitch, Preci-dip, Switzerland) to be compatible with the used headstage (ME2100-HS32-M, Multichannel Systems).

Electrophysiology recording
VFT plants were placed inside a Faraday cage and allowed to acclimate for at least 10 min before the experiments. For NeuroGrid recordings, the NeuroGrid was simply laminated to the outer part of one of the lobes, using small amount of phosphate-buffered saline electrolyte. A Ag/AgCl electrode in the soil was used as the reference electrode. Baseline recordings (no activity) were captured for at least 20 s before stimulation. Different trigger hairs were then mechanically stimulated using a thin metal wire. For nonclosing experiments, each stimulation was performed with at least 1 min interval. For closing experiments, two stimulations were performed within 30 s. For experiments with ionic blockers, either a Ag/AgCl or a FlexMEA72 (Multichannel Systems, Germany) was placed on the inner side of the immobilized trap, being interfaced with Signa gel or in-house fabricated PSSNa hydrogel (4:1:1 mix of PSSNa, d-sorbitol, and glycerol) (*44*), respectively. All experiments were acquired using a ME2100-System (Multichannel Systems, Germany) in DC-coupled mode, with sampling rates from 10 to 50 kHz.

Video acquisition
Video recordings of trap closure were acquired with an area scan camera (acA1280-60gc, Basler AG, Ahrensburg, Germany) with a 6.0 mm lens (FL-CC0614A-2 M - F1.4/6 mm, Ricoh, Tokyo, Japan) at 30 frames/s. Frame acquisition was controlled by a signal generator (InfiniiVision 3000A X-Series, Keysight Technologies, CA, USA), sending a pulse wave of 5 V and a frequency of 30 Hz. This signal was also used to synchronize the video with the electrophysiology setup.

Wound assay
For wound-induced APs, a millisecond-pulsed laser (OFL365-5-TTL3, OdicForce) beam was directed toward the inner side of the trap in a location away from the hairs. The laser beam (wavelength, 450 nm) was operated at a 0.5 W output power using Pulse Width Modulation (PWM), with a pulse width of 1 ms. For optimal wounding, the laser beam of smallest spot size was applied at the region of interest, by properly adjusting the focus. The position of the laser module was fixed with a rigid clamp. The ON duration of the laser beam application was set at 500 ms and controlled by a push button. The laser ON/OFF power switch and the PWM-

modulated laser power controller was custom-designed using an Arduino microcontroller and basic electronic components. The wound size of 1 to 2 mm diameter disk was realized by fixing the height of the laser to 10 cm from the target spot. Thel NeuroGrid was placed on the outer part of the trap to record the wound generated APs.

Pharmacological treatment

Traps were immobilized with double-sided tape on a glass carrier, and the free lobe was excised by the midrib. The exposed lobes were then incubated with different ion channel blocker solutions. For the impairment of Ca^{2+} signaling, plants were incubated with different concentrations of $LaCl_3$ in DI water (10, 50, and 100 mM). For the impairment of K^+ signaling, plants were incubated with different concentrations of TEACl in DI water (10, 50, and 100 mM). Control plants were incubated for the same time with DI water. For the determination of the time-dependent action of the ion channel blockers, APs were recorded every hour with a Ag/AgCl electrode. For the high-resolution mapping, traps were exposed to 10 mM $LaCl_3$ for 3 hours or 10 mM TEACl for 4 hours; at which points, APs were recorded with the FlexMEA72 purchased from Multichannel Systems.

Data analysis

Raw traces obtained from electrophysiology recordings were smoothed with a Savitzky-Golay filter (200 ms window), and their baseline was brought to zero. The timing of the AP at each electrode was determined on the basis of the point of maximum deflection of the signal (local maximum of the derivative). The relative time delay was then calculated as the time difference between each electrode and the first timestamp. Time maps corresponding to the same condition (triggered hair and stimulation number combination) were then spatially aligned by the electrode of origin and averaged, generating the average propagation maps. For these maps, data between electrodes were generated by a cubic interpolation method. Propagation speed was calculated as the slope of a linear fit of the data of all recording electrodes. Regarding phase shift analysis of the AP propagation, phase angle time series of the APs were created using a complex Morlet wavelet with a center frequency of 1.14 Hz, which represents the main frequency content of the AP signal. Following the generation of the phase angle time series, the phase angle difference relative to the origin electrode (first timestamp) was calculated at the FWHM time point. For statistical analysis, at least three independent experiments were performed in different plants. Data were analyzed with custom MATLAB scripts and GraphPad Prism 9. Movement data were extracted from the videos using the software Tracker.

Supplementary Materials
This PDF file includes:
Figs. S1 to S8
Table S1

REFERENCES AND NOTES
1. M. Krausko, Z. Perutka, M. Šebela, O. Šamajová, J. Šamaj, O. Novák, A. Pavlovǐ, The role of electrical and jasmonate signalling in the recognition of captured prey in the carnivorous sundew plant *Drosera capensis*. *New Phytol.* **213**, 1818–1835 (2017).

2. A. G. Volkov, J. C. Foster, K. D. Baker, V. S. Markin, Mechanical and electrical anisotropy in *Mimosa pudica* pulvini. *Plant Signal. Behav.* **5**, 1211–1221 (2010).

3. J. Moe-Lange, N. M. Gappel, M. Machado, M. M. Wudick, C. S. A. Sies, S. N. Schott-Verdugo, M. Bonus, S. Mishra, T. Hartwig, M. Bezrutczyk, D. Basu, E. E. Farmer, H. Gohlke, A. Malkovskiy, E. S. Haswell, M. J. Lercher, D. W. Ehrhardt, W. B. Frommer, T. J. Kleist, Interdependence of a mechanosensitive anion channel and glutamate receptors in distal wound signaling. *Sci. Adv.* **7**, eabg4298 (2021).

4. V. Salvador-Recatalà, W. F. Tjallingii, E. E. Farmer, Real-time, in vivo intracellular recordings of caterpillar-induced depolarization waves in sieve elements using aphid electrodes. *New Phytol.* **203**, 674–684 (2014).

5. S. A. R. Mousavi, A. Chauvin, F. Pascaud, S. Kellenberger, E. E. Farmer, GLUTAMATE RECEPTOR-LIKE genes mediate leaf-to-leaf wound signalling. *Nature* **500**, 422–426 (2013).

6. G. Wang, C. Hu, J. Zhou, Y. Liu, J. Cai, C. Pan, Y. Wang, X. Wu, K. Shi, X. Xia, Y. Zhou, C. H. Foyer, J. Yu, Systemic root-shoot signaling drives jasmonate-based root defense against nematodes. *Curr. Biol.* **29**, 3430–3438.e4 (2019).

7. P. Marhavý, A. Kurenda, S. Siddique, V. Dénervaud Tendon, F. Zhou, J. Holbein, M. S. Hasan, F. M. Grundler, E. E. Farmer, N. Geldner, Single-cell damage elicits regional, nematode-restricting ethylene responses in roots. *EMBO J.* **38**, e100972 (2019).

8. E. E. Farmer, Y.-Q. Gao, G. Lenzoni, J.-L. Wolfender, Q. Wu, Wound- and mechanostimulated electrical signals control hormone responses. *New Phytol.* **227**, 1037–1050 (2020).

9. R. Hedrich, E. Neher, Venus flytrap: How an excitable, carnivorous plant works. *Trends Plant Sci.* **23**, 220–234 (2018).

10. D. Hodick, A. Sievers, The action potential of *Dionaea muscipula* Ellis. *Planta* **174**, 8–18 (1988).

11. S. A. R. Mousavi, C. T. Nguyen, E. E. Farmer, S. Kellenberger, Measuring surface potential changes on leaves. *Nat. Protoc.* **9**, 1997–2004 (2014).

12. A. G. Volkov, C. L. Vilfranc, V. A. Murphy, C. M. Mitchell, M. I. Volkova, L. O'Neal, V. S. Markin, Electrotonic and action potentials in the Venus flytrap. *J. Plant Physiol.* **170**, 838–846 (2013).

13. S. L. Jacobson, Receptor response in Venus's fly-trap. *J. Gen. Physiol.* **49**, 117–129 (1965).

14. S. Scherzer, J. Böhm, S. Huang, A. L. Iosip, I. Kreuzer, D. Becker, M. Heckmann, K. A. S. Al-Rasheid, I. Dreyer, R. Hedrich, A unique inventory of ion transporters poises the Venus flytrap to fast-propagating action potentials and calcium waves. *Curr. Biol.* **32**, 4255–4263.e5 (2022).

15. J. M. T. Bakker, C. N. W. Belterman, R. Coronel, Excitability and propagation of the electrical impulse in Venus flytrap; a comparative electrophysiological study of unipolar electrograms with myocardial tissue. *Bioelectrochemistry* **140**, 107810 (2021).

16. C. G. Bischak, L. Q. Flagg, D. S. Ginger, Ion exchange gels allow organic electrochemical transistor operation with hydrophobic polymers in aqueous solution. *Adv. Mater.* **32**, 2002610 (2020).

17. A. Fabricant, G. Z. Iwata, S. Scherzer, L. Bougas, K. Rolfs, A. Jodko-Władzińska, J. Voigt, R. Hedrich, D. Budker, Action potentials induce biomagnetic fields in carnivorous Venus flytrap plants. *Sci. Rep.* **11**, 1438 (2021).

18. J. Böhm, S. Scherzer, E. Krol, I. Kreuzer, K. Meyer, C. Lorey, T. D. Mueller, L. Shabala, I. Monte, R. Solano, K. A. S. Al-Rasheid, H. Rennenberg, S. Shabala, E. Neher, R. Hedrich, The Venus flytrap *Dionaea muscipula* counts prey-induced action potentials to induce sodium uptake. *Curr. Biol.* **26**, 286–295 (2016).

19. J. O. Stuhlman Jr., E. B. Garden, The action potentials obtained from Venus' flytrap. *Science* **111**, 491–492 (1950).

20. B. Buchen, D. Hensel, A. Sievers, Polarity in mechanoreceptor cells of trigger hairs of *Dionaea muscipula* Ellis. *Planta* **158**, 458–468 (1983).

21. T. Sibaoka, Action potentials and rapid plant movements, in *Plant Growth Substances 1979* (Springer, 1980), pp. 462–469.

22. H. Suda, H. Mano, M. Toyota, K. Fukushima, T. Mimura, I. Tsutsui, R. Hedrich, Y. Tamada, M. Hasebe, Calcium dynamics during trap closure visualized in transgenic Venus flytrap. *Nat. Plants.* **6**, 1219–1224 (2020).

23. A.-L. Iosip, S. Scherzer, S. Bauer, D. Becker, M. Krischke, K. A. S. Al-Rasheid, J. Schultz, I. Kreuzer, R. Hedrich, DYSCALCULIA, a Venus flytrap mutant without the ability to count action potentials. *Curr. Biol.* **33**, 589–596.e5 (2023).

24. P. Jastrzebska-Perfect, S. Chowdhury, G. D. Spyropoulos, Z. Zhao, C. Cea, J. N. Gelinas, D. Khodagholy, Translational Neuroelectronics. *Adv. Funct. Mater.* **30**, 1909165 (2020).

25. E. Song, J. Li, S. M. Won, W. Bai, J. A. Rogers, Materials for flexible bioelectronic systems as chronic neural interfaces. *Nat. Mater.* **19**, 590–603 (2020).

26. M. E. Spira, A. Hai, Multi-electrode array technologies for neuroscience and cardiology. *Nat. Nanotechnol.* **8**, 83–94 (2013).

27. A. R. Hassan, Z. Zhao, J. J. Ferrero, C. Cea, P. Jastrzebska-Perfect, J. Myers, P. Asman, N. F. Ince, G. McKhann, A. Viswanathan, S. A. Sheth, D. Khodagholy, J. N. Gelinas, Translational organic neural Interface devices at single neuron resolution. *Adv. Sci.* **9**, 2202306 (2022).

28. D. Khodagholy, J. N. Gelinas, T. Thesen, W. Doyle, O. Devinsky, G. G. Malliaras, G. Buzsáki, NeuroGrid: Recording action potentials from the surface of the brain. *Nat. Neurosci.* **18**, 310–315 (2015).

29. E. Masi, M. Ciszak, G. Stefano, L. Renna, E. Azzarello, C. Pandolfi, S. Mugnai, F. Baluška, F. T. Arecchi, S. Mancuso, Spatiotemporal dynamics of the electrical network activity in the root apex. *Proc. Natl. Acad. Sci.* **106**, 4048–4053 (2009).

30. D.-J. Zhao, Z.-Y. Wang, L. Huang, Y.-P. Jia, J. Q. Leng, Spatio-temporal mapping of variation potentials in leaves of *Helianthus annuus* L. seedlings in situ using multi-electrode array. *Sci. Rep.* **4**, 5435 (2014).

31. F. Meder, S. Saar, S. Taccola, C. Filippeschi, V. Mattoli, B. Mazzolai, Ultraconformable, self-adhering surface electrodes for measuring electrical signals in plants. *Adv. Mater. Technol.* **6**, 2001182 (2021).

32. W. Li, N. Matsuhisa, Z. Liu, M. Wang, Y. Luo, P. Cai, G. Chen, F. Zhang, C. Li, Z. Liu, Z. Lv, W. Zhang, X. Chen, An on-demand plant-based actuator created using conformable electrodes. *Nat. Electron.* **4**, 134–142 (2021).

33. A. Armada-Moreira, C. Diacci, A. M. Dar, M. Berggren, D. T. Simon, E. Stavrinidou, Bench-marking organic electrochemical transistors for plant electrophysiology. *Front. Plant Sci.* **13**, 916120 (2022).

34. A. G. Volkov, Signaling in electrical networks of the Venus flytrap (*Dionaea muscipula* Ellis). *Bioelectrochemistry* **125**, 25–32 (2019).

35. J. R. Dipalma, R. Mohl, W. Best Jr., Action potential and contraction of *Dionaea muscipula* (Venus flytrap). *Science* **133**, 878–879 (1961).

36. A. G. Volkov, H. Carrell, V. S. Markin, Molecular electronics of the *Dionaea muscipula* trap. *Plant Signal. Behav.* **4**, 353–354 (2009).

37. Y. Forterre, J. M. Skotheim, J. Dumals, L. Mahadevan, How the Venus flytrap snaps. *Nature* **433**, 421–425 (2005).

38. A. Pavlovǐ, J. Jakšová, O. Novák, Triggering a false alarm: Wounding mimics prey capture in the carnivorous Venus flytrap (*Dionaea muscipula*). *New Phytol.* **216**, 927–938 (2017).

39. S. Scherzer, L. Shabala, B. Hedrich, J. Fromm, H. Bauer, E. Munz, P. Jakob, K. A. S. Al-Rascheid, I. Kreuzer, D. Becker, M. Eiblmeier, H. Rennenberg, S. Shabala, M. Bennett, E. Neher, R. Hedrich, Insect haptoelectrical stimulation of Venus flytrap triggers exocytosis in gland cells. *Proc. Natl. Acad. Sci. U.S.A.* **114**, 4822–4827 (2017).

40. S. Scherzer, W. Federle, K. A. S. Al-Rasheid, R. Hedrich, Venus flytrap trigger hairs are micronewton mechano-sensors that can detect small insect prey. *Nat. Plants.* **5**, 670–675 (2019).

41. Y.-Q. Gao, P. Jimenez-Sandoval, S. Tiwari, S. Stolz, J. Wang, G. Glauser, J. Santiago, E. E. Farmer, Ricca's factors as mobile proteinaceous effectors of electrical signaling. *Cell* **186**, 1337–1351.e20 (2023).

42. M. Grenzi, S. Buratti, A. S. Parmagnani, I. A. Aziz, I. Bernacka-Wojcik, F. Resentini, J. Šimura, F. G. Doccula, A. Alfieri, L. Luoni, K. Ljung, M. C. Bonza, E. Stavrinidou, A. Costa, Long-distance turgor pressure changes induce local activation of plant glutamate receptor-like channels. *Curr. Biol.* **33**, 1019–1035.e8 (2023).

43. U. Ricca, Soluzione d'un problema di fisiologia: La propagazione di stimolo nella Mimosa. *Nuovo G. Bot. Ital.* **23**, 51–170 (1916).

44. C.-Y. Yang, D. Tu, T.-P. Ruoko, J. Y. Gerasimov, H.-Y. Wu, C. Harikesh, M. Massetti, M.-A. Stoeckel, R. Kroon, C. Müller, M. Berggren, S. Fabiano, Low-power/high-gain flexible complementary circuits based on printed organic electrochemical transistors. *Adv. Electron. Mater.* **8**, 2100907 (2022).

Science Advances

Plant electrophysiology with conformable organic electronics: Deciphering the propagation of Venus flytrap action potentials

Adam Armada-Moreira, Abdul Manan Dar, Zifang Zhao, Claudia Cea, Jennifer Gelinas, Magnus Berggren, Alex Costa, Dion Khodagholy, and Eleni Stavrinidou

View the article online
https://www.science.org/doi/10.1126/sciadv.adh4443
Permissions
https://www.science.org/help/reprints-and-permissions

Use of this article is subject to the Terms of service